

A Modular Approach to the Embodiment of Hand Motions from Human Demonstrations

Alexander Fabisch¹, Melvin Laux², Dennis Marschner³, Johannes Brust⁴

Abstract—Manipulating objects with robotic hands is a complicated task. Not only the pose of the robot’s end effector, but also the fingers of the hand need to be controlled and coordinated. Using human demonstrations of movements is an intuitive and data-efficient way of guiding the robot’s behavior. We propose a modular framework with an automatic embodiment mapping to transfer human hand motions to robotic systems and use motion capture to record human motion. We evaluate our approach on eight challenging tasks, in which a robotic arm with a mounted robotic hand needs to grasp and manipulate deformable objects or small, fragile material.

I. INTRODUCTION

Although manipulation of known objects is a well-studied field, handling deformable or small, fragile objects with human-level skill is still a challenge. Behaviors for robotic hands can be generated through various approaches, e.g., planning, reinforcement learning, or imitation learning [3], [1], [29]. To leverage intuitive human knowledge, we are interested in generating data for imitation learning with a complex hand. Dataset generation is difficult in this case. Kinesthetic teaching becomes tricky when a 5-finger hand and the end effector’s pose need to be controlled. Teleoperation might not exploit the full potential of the human demonstration due to restricted movement or control difficulties.

We propose to use external sensors (a motion capture system) to track human hands and transfer their states to robotic hands. To do this, we infer the human hand’s state with a record mapping [1]. Next, we solve the correspondence problem [28], induced by kinematic differences between human and robotic hands, with an embodiment mapping [1].

Our goal is to develop a modular framework that allows us to easily replace the sensor and record mapping, as well as the target system (see Figure 1). For example, it should be easy to switch from motion capture to camera-based hand tracking. For this reason, we use the MANO hand model [33], which has previously been used in camera-based hand tracking [20], as an intermediate representation of the hand’s state. The embodiment mapping should also be configurable to handle multiple robotic hands.

The European Commission supported this work through a grant (870142).

¹Alexander Fabisch, Robotics Innovation Center, German Research Center for Artificial Intelligence (DFKI GmbH), Robert-Hooke-Straße 1, D-28359 Bremen, Germany (alexander.fabisch@dfki.de)

²Melvin Laux, Robotics Research Group, University of Bremen (laux@uni-bremen.de)

³Dennis Marschner, Faculty 3 - Mathematics and Computer Science, University of Bremen

⁴Johannes Brust, Plan-Based Robot Control, German Research Center for Artificial Intelligence (DFKI GmbH) (johannes.brust@dfki.de)

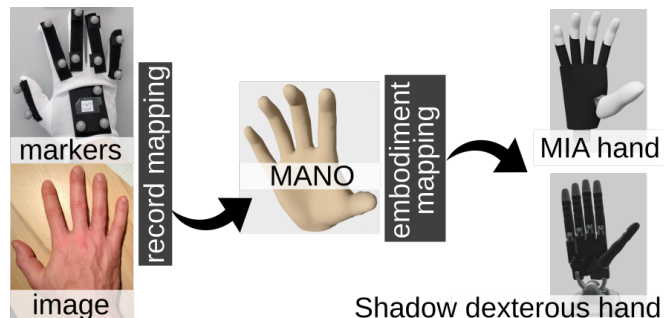


Fig. 1: Proposed approach to embodiment of hand motions.

II. BACKGROUND AND RELATED WORK

A. Motion Capture of Human Hands

Capturing human hand motions as fully articulated 3D hand poses is demanding due to the dexterity of hands, high angular velocities, and many degrees of freedom. Nevertheless, the task is well studied and there are numerous solutions, including optical (markerless or marker-based) and non-optical methods, as well as hybrid and mixed methods.

1) *Non-optical Methods*: Methods based on electromagnetic transmitters [34], [24], [5], bending [15], [35], [7] or stretch-sensors [6], [2], [16], inertial measurement units [26], [21], [10], or even exoskeletons [31] are often integrated as gloves. Caeiro-Rodríguez et al. provide a review of commercial active smart gloves [4]. These methods are suitable for real-time applications, but several problems, such as complex calibration and noisy data with drift over time, remain. Considering different hand shapes, it is not trivial to place multiple sensors perfectly on the glove without loss of accuracy or hand shape-dependent calibration methods.

2) *Optical Methods*: The continuum of optical methods ranges from estimators based on markerless, monocular color images to marker-based motion capture systems using multiple cameras. Markerless methods, mostly based on deep learning, led to groundbreaking progress in computer vision. However, various factors such as lighting conditions, image resolution, background and skin color can influence their performance. Optical markerless approaches can be divided into generative [38], [17] and discriminative methods [45], [27], [30]. Depth information can improve the accuracy of markerless optical methods. However, most methods reach their limits in everyday applications because they generalize insufficiently. Self-occlusion and occlusion when interacting with objects are problems. There are multi-view approaches [39], [40], [41], [36] to minimize these.

For optical marker-based methods, we refer to as motion capture (MOCAP), which is widely used in both the film industry to create realistic animations [43] and for motion analysis in sports biomechanics and rehabilitation [9]. With the proper hardware and environment, professional MOCAP systems estimate hand poses more accurately than non-marker based methods. With a growing number of perspectives and higher camera resolutions, marker detection accuracy, as well as the robustness against occlusions increase. However, such systems are expensive and are of little use outside of laboratories.

3) *Human Hand Pose Models*: Cobos et al. show that 24 DOF are suitable for modeling the high kinematic complexity of human hands during manipulation [8]. Yet, no universal kinematic hand model is equally suitable for all capturing methods, and the number of measurement points varies greatly between different hardware setups. In non-optical methods, labeled 3D joints of hand and finger key points, as well as joint angles, are commonly measured. Optical approaches usually estimate labeled 2.5D or 3D joints, but not joint angles. Mostly, labeled 3D points are assigned to a hand skeleton, which is helpful for advanced applications. However, human hand poses can also be represented as differentiable 3D hand models such as MANO [33], whose surface mesh can be fully deformed and posed. Compared to only regressing a 3D hand skeleton, this 3D hand mesh makes the method immediately usable for computer vision and embodiment mapping.

B. Embodiment Mapping

Embodiment mappings solve the problem of fitting movements demonstrated by a human to a robotic target system. The main challenge of this task is to deal with the differences between kinematic structures and dynamics of humans and robots. Previous works focus on robotic arms [25], [18], [19] and define complex objective functions that have to be solved for a complete trajectory, which makes an immediate embodiment mapping impossible.

We aim to design an embodiment mapping for robotic hands with different properties. We consider individual steps instead of whole motions, which enables us to map each state of the human hand online if it is done fast enough. Hence, the objective can be decoupled into multiple independent problems: one for each finger per step of the motion.

C. Robotic Hands

We consider two robotic hands as target platforms: Prenilia’s Mia Hand, as an example of a simple, robust robotic hand, and the Shadow Dexterous Hand of Shadow Robot Company as an example of a complex, fragile hand.

1) *Mia Hand*: The Mia Hand is a simple, but robust robotic hand with 4 degrees of freedom: thumb adduction/abduction (binary) and flexion, index finger flexion as well as coupled flexion of middle, ring, and little finger, which are controlled by the same motor. As it is not possible to quickly switch between adduction and abduction of the thumb, we consider this joint to be fixed. We can send control commands to the hand at 20 Hz.

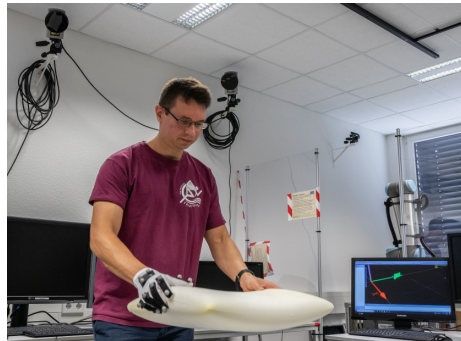


Fig. 2: Motion capture experiment.

2) *Shadow Dexterous Hand*: The Shadow Dexterous Hand is complex as it has 24 DOF, of which 20 are controlled actively. The last two joints of each finger (except the thumb) are coupled, such that the last joint moves when the previous one reaches the joint limit and vice versa. We can send control commands to the hand at 500 Hz.

III. MODULAR RECORD AND EMBODIMENT MAPPING FOR ROBOTIC HANDS

We propose a modular framework to transfer human hand motions to robotic hands. Modularity allows us to easily adapt to new input modalities and target systems.

A. Desiderata

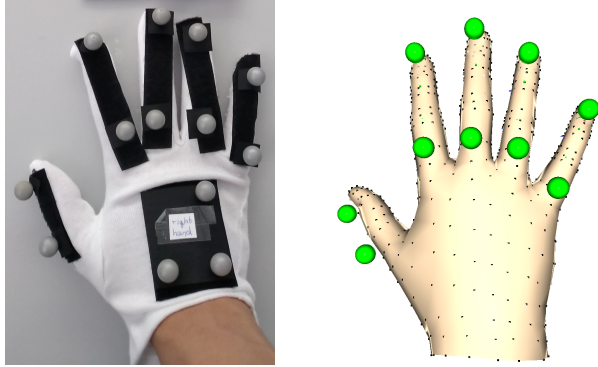
To transfer hand motions demonstrated by humans to a robot, we define a record and an embodiment mapping. We develop an approach that fulfills the following criteria:

- The approach should be adaptable to different input modalities by replacing the record mapping.
- Hence, the result of the record mapping should be a common representation of human hand states.
- The embodiment mapping should be fast enough to not be a bottleneck (at least as fast as the record mapping).
- The embodiment mapping should be able to adapt to the target system through configuration.

B. Record Mapping for Motion Capture System

The objective of the record mapping is to estimate the state of the MANO model from motion capture markers. We use a Qualisys motion capture system and a glove with 13 attached passive markers (see Figure 2) for the right hand. Three markers on the back of the hand can be translated to the hand’s pose and two markers per finger are used to estimate its state (see Figure 3a).

We use colors to distinguish between **estimated or measured quantities** and **configuration parameters** in formulas. To estimate the pose $T_{\text{world,MANO}} \in SE(3)$ (read: active transformation from MANO frame to world frame) of the MANO model, we first derive the pose $T_{\text{world,hand}} \in SE(3)$ of the back of the hand based on three labeled markers. In accordance with the two-vector representation [11], we define the hand frame orientation by the approach vector (direction from right to front hand marker) and the orientation vector (direction orthogonal to the plane defined by



(a) Motion capture glove.

(b) MANO model with expected marker positions indicated by green spheres.

Fig. 3: Mapping from motion capture markers to MANO.

the three markers). The hand’s position can be any point in the plane of the three markers. When we know the fixed transformation $T_{\text{hand,MANO}} \in SE(3)$, we compute

$$T_{\text{world,MANO}} = T_{\text{world,hand}} T_{\text{hand,MANO}}.$$

With the known pose of the MANO model, estimating the finger states boils down to solving five individual optimization problems. We compute each finger’s forward kinematics, $f_{\beta,i,j}(\mathbf{q}) = \mathbf{p}_{i,j}$, for the two points $\mathbf{p}_{i,1}, \mathbf{p}_{i,2}$ (see Figure 3b), where $\mathbf{q}_i \in \mathbb{R}^9$ are the joint angles of finger $i \in \{1, \dots, 5\}$. The resulting optimization problems for each finger are defined as

$$\mathbf{q}_i^* = \arg \min_{\mathbf{q}_i} \sum_{j=1}^2 \|\hat{\mathbf{p}}_{i,j} - f_{\beta,i,j}(\mathbf{q}_i)\|^2 + \|\max(\mathbf{w}_{i,+}^T \mathbf{q}_i, 0)\|^2 + \|\min(\mathbf{w}_{i,-}^T \mathbf{q}_i, 0)\|^2,$$

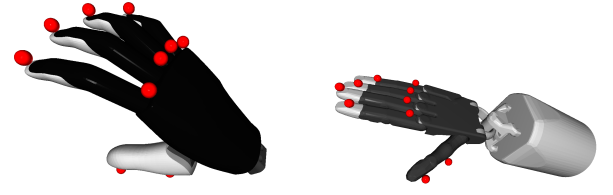
subject to $\mathbf{q}_i^{\min} \leq \mathbf{q}_i \leq \mathbf{q}_i^{\max}$, where $\mathbf{w}_{i,+}, \mathbf{w}_{i,-} \in \mathbb{R}^9$ are weights to penalize each joint angle individually in positive and in negative direction, $\mathbf{q}_i^{\min}, \mathbf{q}_i^{\max} \in \mathbb{R}^9$ are lower and upper bounds for joint angles, and $\beta \in \mathbb{R}^{10}$ are shape parameters of the MANO model. $\hat{\mathbf{p}}_{i,j}$ are measured positions of motion capture markers. We solve these optimization problems with sequential least squares programming (SLSQP, [23]) and numerically estimated gradients.

The MANO model’s full state is defined by $\mathbf{q}_i^* \in \mathbb{R}^9$ and $T_{\text{world,MANO}} \in SE(3)$, from which we can compute the corresponding marker points $\mathbf{p}_{i,j}^* \in \mathbb{R}^3$.

C. Embodiment Mapping

The embodiment mapping translates MANO states to states of the target system, which is a combination of a robotic arm and hand. Assuming that poses are reachable, the robotic hand’s pose first needs to be matched to the mesh pose, i. e., we must define $T_{\text{robot,MANO}} \in SE(3)$.

Next, the individual finger configurations are optimized to be as close as possible to the MANO mesh. Without real-time constraints, the ideal solution is to define an objective



(a) Model of Mia hand with expected marker positions.

(b) Model of Shadow dexterous hand with expected marker positions.

Fig. 4: Extended kinematic hand models.

function to either maximize the overlap between the volumes or to minimize the distance between the inner surfaces of MANO’s fingers and the fingers of the robotic hand. With the intention to be able to transfer motions in real-time, we propose a simplified approach. We define points with respect to the links of the robotic hands (see Figure 4) and minimize the distance to their corresponding virtual markers on the MANO mesh (see Figure 3b), for which the positions are known from the record mapping.

Thus, the optimization of finger joints reduces to an inverse kinematics problem, in which only the distance between two pairs of points per finger i is minimized:

$$\mathbf{r}_i^* = \arg \min_{\mathbf{r}_i} \sum_{j=1}^2 \|f_{\beta,i,j}(\mathbf{q}_i^*) - g_{i,j}(\mathbf{r}_i)\|^2,$$

subject to $\mathbf{r}_i^{\min} \leq \mathbf{r}_i \leq \mathbf{r}_i^{\max}$. $f_{\beta,i,j}(\mathbf{q}_i^*)$ is known from record mapping and $g_{i,j}(\mathbf{r}_i)$ is the corresponding forward kinematics function for the robotic hand with the joint angles $\mathbf{r}_i \in \mathbb{R}^{N_i}$ and limits $\mathbf{r}_i^{\min}, \mathbf{r}_i^{\max} \in \mathbb{R}^{N_i}$. The number of optimized joints $N_i \in \mathbb{N}$ depends on the target system, as e.g., the Mia hand’s index finger is controlled by a single motor while the Shadow dexterous hand uses three motors to control the index finger. Once again, we use SLSQP to solve the optimization problem.

D. Configuration

While we assume well-defined kinematics, it is necessary to configure certain parameters of the record and embodiment mapping. For this work, these parameters were configured manually, however, this could potentially be partially automated. For instance, a black-box optimizer could optimize the shape parameters for the MANO model to fit motion capture markers.

For the record mapping, we need to configure:

- $T_{\text{hand,MANO}} \in SE(3)$: transformation between MANO base and hand coordinate frame defined by three motion capture markers at the back of the hand
- $\beta \in \mathbb{R}^{10}$: shape parameters of MANO
- $\mathbf{w}_{i,+}, \mathbf{w}_{i,-} \in \mathbb{R}^9$: weights to penalize each joint angle individually in both directions
- $\mathbf{q}_i^{\min}, \mathbf{q}_i^{\max} \in \mathbb{R}^9$: joints’ lower and upper bounds

For the embodiment mapping, we need to configure

- $T_{\text{robot,MANO}} \in SE(3)$: transformation between the MANO mesh’s and the robotic hand’s bases

Task	Variations	Demonstrations
Grasp insole	from front or back	213
Insert insole	-	12
Grasp small pillow	from four sides	224
Grasp big pillow	from four sides	130
Grasp electronic component	from all sides	55
Assemble electronic components	from all directions	54
Flip pages	-	38
Insert passport in box	-	37
Total		763

TABLE I: Overview of datasets used for evaluation.



Fig. 5: Objects used to record datasets. Left to right and top to bottom: insole with markers, insole and bag, small pillow with markers, open passport, passport and box, electronic components with markers.

- expected marker positions (see Figure 4) with respect to corresponding frames in the hand’s kinematic tree

IV. EVALUATION

A. Research Question

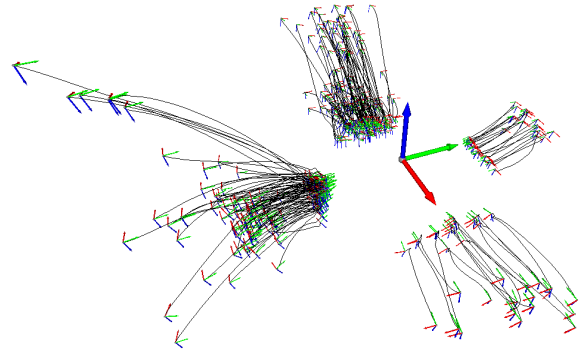
It has been shown that the state of the MANO model can be obtained from RGB images [20]. Our goal is to show that

- 1) It is possible to obtain the MANO representation from motion capture data.
- 2) The embodiment mapping can be easily adapted to both robotic hands.
- 3) The embodiment mapping obtains plausible corresponding configurations of the robotic hand even when the target system has less DOF than a human hand.
- 4) The transferred trajectories result in a physically verified useful behavior of the target systems.
- 5) Both record and embodiment mapping can be executed at a frequency that can be used for teleoperation.

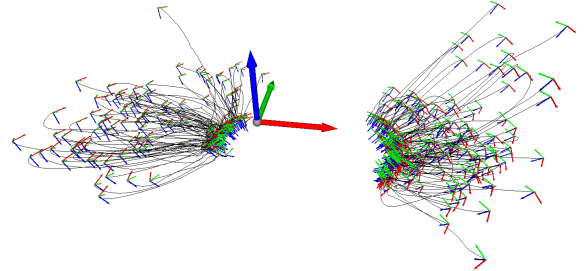
B. Datasets

To evaluate the hand embodiment mapping, we recorded demonstrations of multiple tasks, variations of these, and repetitions as summarized in Table II with a Qualisys motion capture system.¹ Objects that were used during these experiments are shown in Figure 5 and visualizations of the end-effector trajectories in Figure 6.

¹Only one subject was recorded because of COVID-19. We argue that this is sufficient since parameters of the record mapping are tuned manually.



(a) Dataset of 224 grasps for a small pillow.



(b) Dataset of 213 grasps for an insole.

Fig. 6: Two of the datasets used for evaluation. Object-relative trajectories of the end effector are represented by lines and coordinate frames that indicate the orientation at the beginning and end. The large coordinate frames in the middle define object poses.

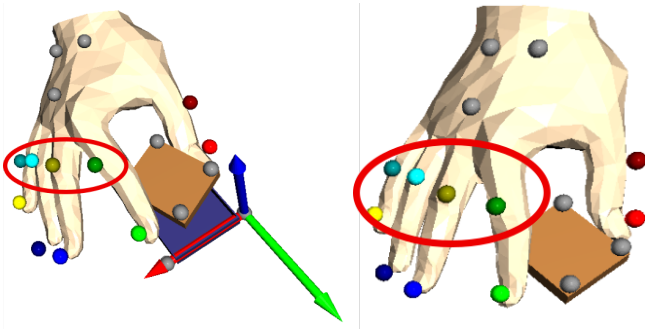
C. Estimation of MANO State (Qualitative Evaluation)

Marker positions were tracked with an error of about 1 mm. These represent the ground truth information for the record mapping, which we need to evaluate the quality of the estimated MANO states. Figure 7 shows exemplary measurements of the motion capture markers with corresponding estimations of the MANO model by the record mapping from marker positions. Differences between the MANO state and the real hand mainly stem from inaccuracies of the MANO configuration: shape and relative transformation of the marker frame spanned by three markers at the back of the hand and their actual placement on the hand. This also varies between experiments and even within individual recordings.

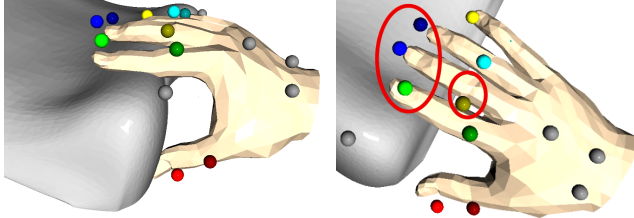
Obvious differences between the estimated MANO state and the actual hand state can be seen, e.g., in Figure 7a (red ellipses): while the marker positions are closer to the metacarpophalangeal joint of the real hand (see Figure 3a), they are closer to the proximal interphalangeal joint of the estimated MANO state.

Furthermore, we can see in Figure 7b (red ellipses) that the lengths of the fingers do not always match the corresponding marker positions. In the same example, the marker close to the metacarpophalangeal joint of the middle finger is laterally shifted, which was actually the case because the marker was not aligned perfectly at the center of the finger.

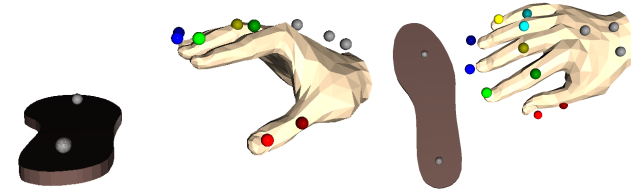
Apart from that, we can see in Figure 7 that the estimated MANO states are mostly plausible explanations of the mea-



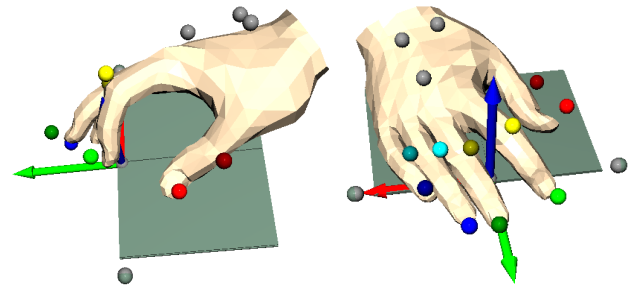
(a) Grasping and assembling electronic components.



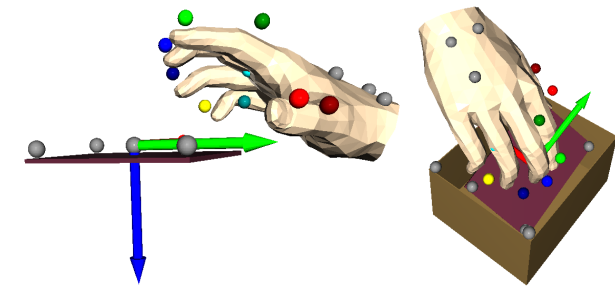
(b) Grasping a small pillow.



(c) Grasping an insole.



(d) Flipping the page of a passport.



(e) Grasping a passport and putting it in a box.

Fig. 7: Exemplary configurations of MANO mesh after record mapping and corresponding motion capture markers. Simplified meshes that illustrate the position of the manipulated objects are displayed with the markers that we used to track their pose. For some objects we also see the object frame. Illustrations were made with Open3D [44].

sured marker positions.

D. Adaptability to Robotic Hand (Qualitative Evaluation)

Figure 8 shows the result of an interactive embodiment mapping. A GUI application was used to set the 48 joint parameters of the MANO model. The embodiment mapping determines joint angles of the robotic hand. Both the MANO mesh and the configuration of the robotic hand are visualized.

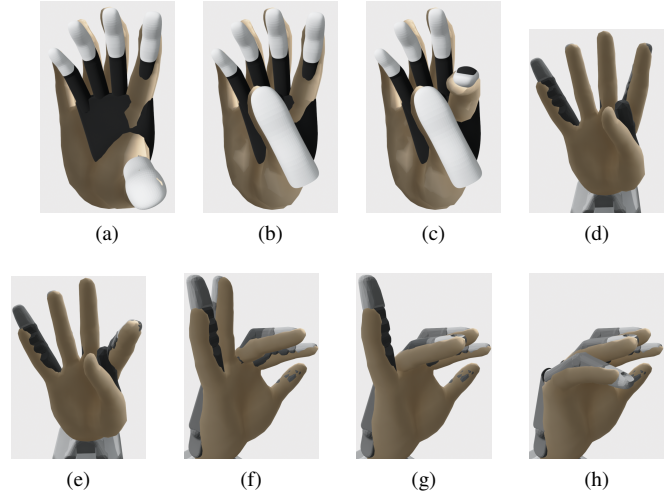


Fig. 8: Interactive embodiment mapping. MANO state and robotic hand after embodiment mapping are displayed together. This visualization is based on Open3D's visualizer [44] and pytransform3d [14].

Figure 8 shows exemplary configurations of the Mia hand (a – c) and configurations of the Shadow dexterous hand (d – h). There are differences between the MANO mesh and the robotic hand that the embodiment mapping cannot compensate for. The Mia hand is slightly smaller than the MANO mesh so that the little fingers cannot be aligned perfectly, while the little finger of the Shadow dexterous hand is longer than the middle finger of the MANO mesh. The Mia hand has only four degrees of freedom, which results in less accurate embodiment, in particular when the middle finger, ring finger, and little finger have a different flexion as these move jointly in the Mia hand. There are also differences that occur due to an inadequate objective: the Shadow dexterous hand is able to minimize the positional difference between the finger tips without having the correct orientation (see Figure 8d) and as long as the tip positions are reached it does not matter whether the joint angles are similar (e.g., see Figure 8h). As it will become apparent in Sections IV-E and IV-G, the last point is the price that we pay to for real-time control of a robotic hand.

E. Similarity Between MANO and Robotic Hand

We compare the inner surface of the fingers of the robotic hand to the MANO mesh to evaluate the embodiment mapping. Hence, we define the contact surfaces of the MANO model and each robotic hand for each finger

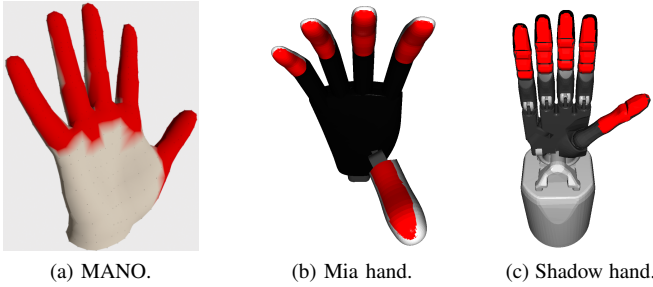


Fig. 9: Contact surfaces of the MANO model and the robotic hands are marked in red color.

Task	Mia hand				
	Thumb	Index	Middle	Ring	Little
Grasp insole	19.2	4.8	11.7	20.7	26.7
Insert insole	6.0	10.3	19.4	24.3	24.7
Grasp small pillow	8.6	9.3	13.4	16.6	24.8
Grasp big pillow	6.4	6.8	13.9	22.8	31.7
Grasp electronic component	7.0	13.2	35.2	38.3	44.9
Assemble electronic components	7.1	13.4	35.1	38.1	44.8
Flip pages	21.5	10.0	23.9	27.5	28.7
Insert passport in box	22.4	10.5	27.8	32.3	38.4

Task	Shadow dexterous hand				
	Thumb	Index	Middle	Ring	Little
Grasp insole	5.2	12.2	6.8	7.5	11.3
Insert insole	4.8	4.2	5.8	5.2	6.7
Grasp small pillow	5.3	3.9	4.6	5.6	10.8
Grasp big pillow	4.6	4.0	5.5	4.6	6.7
Grasp electronic component	5.2	3.5	4.8	5.1	9.0
Assemble electronic components	5.2	3.5	4.8	5.2	9.0
Flip pages	6.1	3.6	4.9	5.3	9.1
Insert passport in box	5.4	6.0	7.2	7.1	9.1

TABLE II: Mean average distance (unit: mm) of contact surfaces. One frame per demonstration was selected.

that we want to compare (see Figure 9). During evaluation, we draw 100 points from the contact surface of each finger of the robotic hand by Poisson disk sampling [42], compute the minimum distance to the closest triangle of the corresponding contact surface of the MANO mesh per sample, and average these minimum distances over all sampled points per finger. More precisely, we compute $\frac{1}{N} \sum_{i=1}^N \min_{j \in \{1, \dots, M\}} d(\mathbf{p}_i, \{\mathbf{q}_{j,1}, \mathbf{q}_{j,2}, \mathbf{q}_{j,3}\})$, where $d(\mathbf{p}, T)$ is the distance between a point and a triangle defined by a set of three points [13], \mathbf{p}_i are points on the contact surface of the robotic finger, $\mathbf{q}_{j,1}, \mathbf{q}_{j,2}, \mathbf{q}_{j,3}$ are points that define a triangle of the contact surface of the corresponding finger of the MANO model, N is the number of samples from the contact surface of the robotic hand, and M is the number of triangles on the contact surface of the MANO mesh. The result is an average distance between the two surfaces. This evaluation is considerably slower than the embodiment. Hence, we only compute it for selected cases.

Table II summarizes the results. It is clear that more

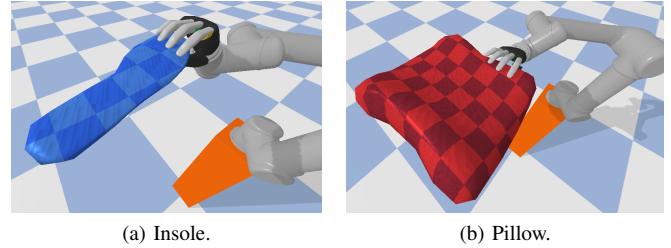


Fig. 10: Simulation environments with UR5 and Mia hand.

degrees of freedom enable the embodiment mapping to fit the desired positions more closely. The Mia hand particularly has problems with fitting the middle, ring and little fingers because they are controlled by only one motor and move together. Furthermore, the Mia hand is slightly smaller than the MANO mesh in the used configuration, as seen in Figure 8. With this transformation between MANO and the base of the robotic hand, however, it is easier to fit the thumb and the index finger accurately.

F. Simulation of Transferred Movements

PyBullet [12] is one of the few physics engines that support robotics and deformable objects. We use it to verify physical plausibility of transferred motions. Since setting up realistic simulation environments and modeling deformable objects that have complex shapes is difficult, we focus on the tasks of grasping an insole and the small pillow.

1) *Objects*: Insoles and pillows are deformable. We model them as homogeneous objects with the stable Neo-Hookean model [37] for hyperelastic material. For the insole we set Young’s modulus to $E = 100$ kPa and Poisson’s ratio to $\nu = 0.2$. For the pillow we set $E = 10$ kPa and $\nu = 0.2$.

2) *Simulation environment*: We test whether the object can be held after the execution of each grasp by simulating the effect of gravity. In our simulation, the objects float in front of the manipulator (see Figure 10). After each completed grasp, we evaluate its success by allowing the object to fall from gravitational force. We continue the simulation for an additional second, after which we measure whether the object is still within the hand.

3) *Grasp quality measures*: Furthermore, we compute grasp quality measures [32]. Among these, we tested force closure, the orthogonality metric, shape and area of the grasp polygon, distance between centroid and center of grasp polygon, wrench resistance and the Ferrari-Canny L1 metric. These metrics are calculated from contact forces and positions of the contact points between hand and grasped object. PyBullet provides these information based on a Finite Element Method simulation of the deformable object. We found, however, that the metrics could not accurately predict the stability of the grasps before grasping, because contact point positions and forces are dynamically changing due to the object’s deformations under gravity and contact forces. After all, these metrics were designed for rigid objects and less human-like robotic grippers. Deformability makes the

evaluation of grasps more complex and requires suitable simulation engines. Therefore, metrics for grasps of deformable objects came into research focus only recently (e.g., [22]) and still have a high barrier for use as an evaluation tool.

4) *Results*: Table III shows the success rate of the embodiment mapping for each combination of task and hand. Considering morphological differences between the human hand and the robotic hands, a success rate of 50 % is a good result, since no sensor feedback is used and the transferred trajectory is simply replicated in simulation. Modifying the trajectory slightly by closing the fingers of the hand further, scaling the size of the object by a factor of 1.1 (equivalent to scaling the trajectory), or both, improves the success rate considerably. Both the insole and the pillow will be grasped on one side, which gives gravity a long lever to generate forces that let the object fall out of the hand. Adding another hand to support the grasp operation would make the solution more robust.

Despite resembling MANO states more faithfully, the Shadow hand does not perform better than the Mia hand in these grasping tasks. We attribute this to the fact that it is not necessary to have many DOF to match the recorded human pinch grasps. In fact, the geometry of the Mia hand is better suited to grasp these two objects firmly than the Shadow hand, mainly due to its bigger thumb.

Object	Samples	Hand	Success Rate			
			Default	Scaled	Closing	Both
Insole	213	Mia	37.6%	53.5%	62.0%	-
		Shadow	29.6%	54.9%	31.5%	61.0%
Small pillow	224	Mia	29.5%	47.3%	65.2%	-
		Shadow	24.6%	59.4%	37.1%	64.3%

TABLE III: Success rates of simulated grasps.

G. Real-Time Control Capabilities

One intended use case of the embodiment mapping is to enable real-time control of a robotic arm and hand through a motion capture system. This allows the operator to compensate for differences of their hand and the robotic hand during execution. A limiting factor here is the frequency at which we receive hand states from the motion capture system, which is 100 Hz. We must generate commands for the robotic hand from motion capture with a similar frequency.

Therefore, we evaluated the frequency at which we can compute the record and embodiment mapping (see Table IV). While the lowest frequencies for both, record and embodiment mapping, prevent real time control even with a control frequency of 20 Hz for the Mia hand, the average frequency of the embodiment mapping is well above the frequency at which the motion capture system provides measurements. However, the record mapping is often too slow for 100 Hz. Nevertheless, in a setup with a Universal Robot that is controlled at 125 Hz and a Mia hand that is controlled at 20 Hz, we can compute the end-effector poses for the arm at a higher frequency, as this is not

computationally demanding, and provide the computationally demanding finger configurations at a lower frequency so that real-time control is possible.

V. CONCLUSIONS

In addition to introducing a modular framework to transfer human hand motions to robotic hands, this work proposes a novel approach to estimate the MANO state with a marker-based motion capture system and a configurable embodiment mapping that is easily adaptable to new robotic hands and simple enough to be fast even for complex robotic hands. Advantages of using a motion capture system include high-precision, low-variance hand pose estimates and accurate measurements of the finger-tips' cartesian positions compared to estimates from single camera images. In addition, using a motion capture system allows for more complex, natural hand and finger motions than kinesthetic teaching.

Transferred motions can initialize, e.g., reinforcement learning, which considerably reduces the necessary exploration for reinforcement learning and makes transferred motions more robust. The evaluation shows promising results in terms of similarity of transferred hand states as well as enough speed for real-time performance, which enables teleoperation of robotic hands.

ETHICS APPROVAL

Experimental protocols were approved by the ethics committee of the University of Bremen. Written informed consent was obtained from all participants.

ACKNOWLEDGMENT

We thank Oscar Lima, Andrea Burani, and Francesca Cini for the URDF of the Mia hand and Lisa Gutzeit for her feedback on the manuscript. The motion capture setup was developed in collaboration with Lisa Gutzeit, supported by a grant from the German Federal Ministry for Economic Affairs and Energy (BMW, FKZ 50 RA 2023).

REFERENCES

- [1] B. D. Argall, S. Chernova, M. Veloso, and B. Browning. A survey of robot learning from demonstration. *Robotics and Autonomous Systems*, 57(5):469–483, 2009.
- [2] A. Atalay, V. Sanchez, O. Atalay, D. Vogt, F. Haufe, R. Wood, and C. Walsh. Batch fabrication of customizable silicone-textile composite capacitive strain sensors for human motion tracking. *Advanced Materials Technologies*, 2, 07 2017.
- [3] A. Billard, S. Calinon, R. Dillmann, and S. Schaal. Robot programming by demonstration. In B. Siciliano and O. Khatib, editors, *Springer Handbook of Robotics*, pages 1371–1394. Springer, Berlin, Heidelberg, 2008.
- [4] M. Caeiro-Rodríguez, I. Otero-González, F. A. Mikic-Fonte, and M. Llamas-Nistal. A systematic review of commercial smart gloves: Current status and applications. *Sensors*, 21(8), 2021.
- [5] K.-Y. Chen, S. Patel, and S. Keller. Finexus: Tracking precise motions of multiple fingertips using magnetic sensing. pages 1504–1514, 2016.
- [6] J.-B. Chossat, Y. Tao, V. Duchaine, and Y.-L. Park. Wearable soft artificial skin for hand motion detection with embedded microfluidic strain sensing. In *ICRA*, pages 2568–2573, 2015.
- [7] S. Ciotti, E. Battaglia, N. Carbonaro, A. Bicchi, A. Tognetti, and M. Bianchi. A synergy-based optimally designed sensing glove for functional grasp recognition. *Sensors (Basel, Switzerland)*, 16, 2016.
- [8] S. Cobos, M. Ferre, M.A. Uran, J. Ortego, and C. Peña Cortés. Efficient human hand kinematics for manipulation tasks. pages 2246–2251, 2008.

Dataset	Frames	Record mapping			Embodiment mapping (Mia)			Embodiment mapping (Shadow)		
		Frequency in Hz								
		average	min	max	average	min	max	average	min	max
Grasp insole	42,285	99.7	5.1	123.2	228.0	15.0	328.6	178.7	0.7	202.2
Insert insole	3,878	82.9	6.2	112.2	280.5	73.2	313.3	162.2	8.5	201.1
Grasp small pillow	31,020	65.8	5.9	126.1	261.1	102.2	322.6	136.7	9.0	204.6
Grasp big pillow	6,945	58.7	5.6	115.1	268.7	97.0	322.4	131.2	8.3	203.5
Grasp electronic component	9,459	84.1	7.2	129.7	292.2	131.0	332.5	169.1	8.6	207.8
Assemble electronic components	16,984	95.2	7.7	121.3	293.9	123.1	328.7	180.7	10.5	212.3
Flip pages	15,484	63.4	9.1	124.1	263.1	108.5	341.7	128.0	0.7	218.4
Insert passport in box	6,669	58.2	3.0	109.6	158.6	16.5	304.3	142.7	8.1	202.9

TABLE IV: Evaluation of speed. Results are statistics of each frame of each demonstration of the corresponding skill. All computations are done by a single core of an AMD Ryzen 7 2700 processor.

- [9] S. L. Colyer, M. Evans, D. P. Cosker, and A. I. T. Salo. A review of the evolution of vision-based motion analysis and the integration of advanced computer vision methods towards developing a markerless system. *Sports Medicine - Open*, 4(1):24, 2018.
- [10] J. Connolly, B. O’Flynn, J. Torres Sanchez, J. Condell, K. Curran, P. Gardiner, and B. Downes. Integrated smart glove for hand motion monitoring. 01 2015.
- [11] P. Corke. *Robotics, Vision and Control*. Springer, 2017.
- [12] E. Coumans and Y. Bai. PyBullet, a python module for physics simulation for games, robotics and machine learning. <http://pybullet.org>, 2016–2022.
- [13] C. Ericson. *Real-Time Collision Detection*. CRC Press, 2004.
- [14] A. Fabisch. pytransform3d: 3d transformations for python. *Journal of Open Source Software*, 4(33):1159, 2019.
- [15] R. Gentner and J. Classen. Development and evaluation of a low-cost sensor glove for assessment of human finger movements in neurophysiological settings. *Journal of Neuroscience Methods*, 178:138–147, 2009.
- [16] O. Glauser, S. Wu, D. Panozzo, O. Hilliges, and O. Sorkine-Hornung. Interactive hand pose estimation using a stretch-sensing soft glove. *ACM Trans. Graph.*, 38(4), jul 2019.
- [17] J. Gu, Z. Wang, W. Ouyang, W. Zhang, J. Li, and L. Zhuo. 3d hand pose estimation with disentangled cross-modal latent space. In *Proceedings of the IEEE/CVF Winter Conference on Applications of Computer Vision (WACV)*, March 2020.
- [18] L. Gutzeit, A. Fabisch, M. Otto, J. H. Metzen, J. Hansen, F. Kirchner, and E. A. Kirchner. The besman learning platform for automated robot skill learning. *Frontiers in Robotics and AI*, 5:43, 2018.
- [19] L. Gutzeit, A. Fabisch, C. Petzoldt, H. Wiese, and F. Kirchner. Automated robot skill learning from demonstration for various robot systems. In Christoph Benzmüller and Heiner Stuckenschmidt, editors, *KI: Advances in Artificial Intelligence*, pages 168–181. Springer, 2019.
- [20] Y. Hasson, G. Varol, D. Tzionas, I. Kalevatykh, M. J. Black, I. Laptev, and C. Schmid. Learning joint reconstruction of hands and manipulated objects. In *CVPR*, 2019.
- [21] P.-C. Hsiao, S.-Y. Yang, B.-S. Lin, I.-J. Lee, and W. Chou. Data glove embedded with 9-axis imu and force sensing sensors for evaluation of hand function. In *Annual International Conference of the IEEE Engineering in Medicine and Biology Society*, pages 4631–4634, 2015.
- [22] I. Huang, Y. S. Narang, C. Eppner, B. Sundaralingam, M. Macklin, T. Hermans, and D. Fox. DefGraspSim: Simulation-based grasping of 3D deformable objects, 2021.
- [23] D. Kraft. A software package for sequential quadratic programming. Technical Report DFLVR-FB 88-28, DLR German Aerospace Center – Institute for Flight Mechanics, Köln, Germany, 1988.
- [24] Y. Ma, Z.-H. Mao, W. Jia, C. Li, J. Yang, and M. Sun. Magnetic hand tracking for human-computer interface. *IEEE Transactions on Magnetics*, 47(5):970–973, 2011.
- [25] G. Maeda, M. Ewerton, D. Koert, and J. Peters. Acquiring and generalizing the embodiment mapping from human observations to robot skills. *IEEE Robotics and Automation Letters*, 1(2):784–791, 2016.
- [26] T. Mańkowski, J. Tomczyński, and P. Kaczmarek. Cie-dataglove, a multi-imu system for hand posture tracking. pages 268–276, 03 2017.
- [27] F. Mueller, F. Bernard, O. Sotnychenko, D. Mehta, S. Sridhar, D. Casas, and C. Theobalt. Generated hands for real-time 3d hand tracking from monocular rgb. In *CVPR*, June 2018.
- [28] C. L. Nehaniv and K. Dautenhahn. *The Correspondence Problem*, pages 41–61. MIT Press, Cambridge, MA, USA, 2002.
- [29] T. Osa, J. Pajarinen, G. Neumann, J. A. Bagnell, P. Abbeel, and J. Peters. An algorithmic perspective on imitation learning. *Foundations and Trends in Robotics*, 7(1–2):1–179, 2018.
- [30] P. Panteleris, I. Oikonomidis, and A. A. Argyros. Using a single RGB frame for real time 3d hand pose estimation in the wild. *CoRR*, abs/1712.03866, 2017.
- [31] A. Pereira, G. Stillfried, T. Baker, A. Schmidt, A. Maier, B. Pleintinger, Z. Chen, T. Hulin, and N. Y. Lii. Reconstructing human hand pose and configuration using a fixed-base exoskeleton. In *ICRA*, pages 3514–3520, 2019.
- [32] M. A. Rao and R. Suarez. Grasp quality measures: review and performance. *Autonomous Robots*, 38(1):65–88, 2015.
- [33] J. Romero, D. Tzionas, and M. J. Black. Embodied hands: Modeling and capturing hands and bodies together. *ACM Transactions on Graphics, (Proc. SIGGRAPH Asia)*, 36(6), November 2017.
- [34] H.-M. Shen, C. Lian, X.-W. Wu, F. Bian, P. Yu, and G. Yang. Full-pose estimation using inertial and magnetic sensor fusion in structured magnetic field for hand motion tracking. *Measurement*, 170:108697, 2021.
- [35] Z. Shen, J. Yi, X. Li, L. H. P. Mark, Y. Hu, and Z. Wang. A soft stretchable bending sensor and data glove applications. In *IEEE International Conference on Real-time Computing and Robotics (RCAR)*, pages 88–93, 2016.
- [36] T. Simon, H. Joo, I. Matthews, and Y. Sheikh. Hand keypoint detection in single images using multiview bootstrapping, 2017.
- [37] B. Smith, F. De Goes, and T. Kim. Stable neo-hookean flesh simulation. *ACM Trans. Graph.*, 37(2), 2018.
- [38] A. Spurr, J. Song, S. Park, and O. Hilliges. Cross-modal deep variational hand pose estimation. *CoRR*, abs/1803.11404, 2018.
- [39] S. Sridhar, A. Oulasvirta, and C. Theobalt. Interactive markerless articulated hand motion tracking using rgb and depth data. In *ICCV*, 2013.
- [40] D. Tzionas, L. Ballan, A. Srikantha, P. Aponte, M. Pollefeys, and J. Gall. Capturing hands in action using discriminative salient points and physics simulation. *CoRR*, abs/1506.02178, 2015.
- [41] R. Wang, S. Paris, and J. Popović. 6d hands: Markerless hand-tracking for computer aided design. In *Proceedings of the 24th Annual ACM Symposium on User Interface Software and Technology*, UIST ’11, page 549–558, New York, NY, USA, 2011. ACM.
- [42] C. Yuksel. Sample elimination for generating poisson disk sample sets. *Computer Graphics Forum (Proceedings of EUROGRAPHICS)*, 34(2):25–32, 2015.
- [43] M. Y. Zhang. Application of performance motion capture technology in film and television performance animation. In *Instruments, Measurement, Electronics and Information Engineering*, volume 347 of *Applied Mechanics and Materials*, pages 2781–2784. Trans Tech Publications Ltd, 10 2013.
- [44] Q.-Y. Zhou, J. Park, and V. Koltun. Open3D: A modern library for 3D data processing, 2018.
- [45] C. Zimmermann and T. Brox. Learning to estimate 3d hand pose from single rgb images. In *ICCV*, 2017. <https://arxiv.org/abs/1705.01389>.